

1 Diagnosis of pulmonary infarction in post-mortem computed tomography
2 and post-mortem magnetic resonance imaging - a technical note.

3

4 Nicolas Herr¹, Paolo Lombardo^{1,2}, Christian Jackowski¹, Wolf Dieter Zech¹

5 1 Institute of Forensic Medicine, University of Bern, Bühlstrasse 20, 3012 Bern Switzerland

6 2 Department of Diagnostic, Interventional and Pediatric Radiology, University of Bern, Inselspital,
7 Freiburgstrasse 10, Bern CH-3010, Switzerland

8

9

10 **Keywords**

11 pulmonary infarction, pulmonary thromboembolism, post-mortem computed
12 tomography, post-mortem magnetic resonance imaging

13

14 **Abstract**

15 Pulmonary thromboembolism may be accompanied by pulmonary infarction. Even
16 though pulmonary thromboembolism (PTE) is a frequently found cause of death at
17 autopsy, pulmonary infarction accompanying PTE is a less common finding and may
18 therefore easily be misinterpreted as infectious or cancerous lung disease.
19 Appearance of pulmonary infarction in post-mortem imaging and acquisition
20 parameters helping to identify pulmonary infarctions are not described yet. Based on
21 a case of a 50-year-old man who died due to PTE and presented pulmonary infarction
22 we suggest using a pulmonary algorithm in post-mortem computed tomography
23 combined with post-mortem magnetic resonance imaging of the lungs using
24 conventional T1 and T2 weighted sequences.

25 **Introduction**

26 We present post-mortem imaging and autopsy results of a 50-year-old man who died
27 from right cardiac failure due to PTE. Post-mortem imaging comprised whole body
28 unenhanced post-mortem computed tomography (PMCT) and unenhanced post-
29 mortem magnetic resonance imaging (PMMR) of the chest prior to forensic autopsy.
30 PM-imaging revealed pulmonary findings suspicious of pulmonary infarction.

1 **Methods and results**

2 **Post-mortem imaging (PMCT and PMMR)**

3 The interval between death and PMCT was 5 hours. Whole body unenhanced PMCT
4 imaging was performed as part of the routine forensic examination using a Siemens
5 Somatom Definition AS 64. Tube voltage was 140 kV, caredose, slice thickness 1 mm,
6 increment 0.7 mm, a rotation time of 0.5 s and a field of view of 570 mm. Soft tissue
7 algorithm and bone tissue algorithm were used. The thorax was reconstructed using a
8 specific pulmonary algorithm with a field of view of 332 mm.

9 PMMR of the thorax was conducted immediately after PMCT. Body temperature at the
10 time of scanning was 23 °C. For PMMR (Philips Achiva 3T) imaging the body was
11 placed in an artifact-free body bag. The applied sequences were T2-weighted
12 sequences (T2_Dixon_tra; slice thickness: 3mm, GAP: 0.3mm, TR: 3957ms, TE:
13 90ms, NSA: 2 and T2_Dixon_cor; slice thickness: 3mm, GAP: 0.3mm, TR: 3957ms,
14 TE: 90ms, NSA: 2) as well as T1-weighted sequences (T1_Dixon_tra; slice thickness:
15 3mm, GAP: 0.3mm, TR: 702ms, TE: 7.39ms, NSA: 1 and T1_Dixon_cor; slice
16 thickness: 3mm, GAP: 0.3mm, TR: 702ms, TE: 7.44ms, NSA: 1). Dixon technique was
17 chosen according to our standard PMMR-protocol allowing to obtain water only, fat
18 only as well as in-phase and out-of-phase images in a single acquisition. PMMR
19 examination time was 25 minutes. All images (PMCT and PMMR) were viewed and
20 evaluated in a PACS (Sectra Workstation IDS7, Version 17.1.16.3569,
21 Linköping/Sweden) by a board-certified radiologist experienced in post-mortem
22 imaging.

23

24

25

1 **Postmortem imaging results**

2 PMCT and PMMR showed three wedge-shaped, pleura-based lesions in the lung
3 periphery (one lesion in the upper right lobe, approx. 29 mm x 22 mm x 31 mm, and
4 two in the lower right lobe, approx. 25 mm x 21.5 mm x 26 mm and 40 mm x 29 mm x
5 38 mm, respectively). Lesions appeared mainly hyperdense with smaller hypodense
6 areas in PMCT (Fig. 1). In PMMR lesions appeared mainly hypointense to isointense
7 containing focal hypointense areas in T1w and mainly hyperintense with focal
8 hypointense areas in T2w in-phase images (Fig. 1). Appearance of pulmonary lesions
9 in Dixon water only, fat only and out-of-phase images is shown in Table 1. Additionally,
10 homogeneous material of intermediate signal intensity within the large and small
11 pulmonary arteries of both lungs compatible with PTE was found in T2w PMMR [1].

12 **Autopsy and Histology**

13 Autopsy was conducted immediately after imaging by board-certified forensic
14 pathologists according to the Recommendation of the Committee of Ministers to
15 Member States of Europe on the harmonization of medico-legal autopsy rules [2] and
16 included external and internal examination with opening of all three body cavities and
17 dissection of all organs. During autopsy tissue samples of the lung as well as tissue
18 samples from all other internal organs were collected for histologic examination.
19 Histology staining included hematoxylin and eosin (H&E) and iron (Fe) staining.
20 Histologic examinations and adjudication were performed by board-certified forensic
21 pathologists. Toxicological examinations were not commissioned by the prosecutor.

22 **Autopsy and histology findings**

23 External examination showed signs of upper venous congestion with livid discoloration
24 of the face, neck and upper chest as well as a visible engorgement of the jugular veins.
25 Internal examination revealed thromboembolic occlusion of the large and small

1 pulmonary arteries of both lungs, partially attached to the vessel walls. Wedge-shaped
2 lesions seen in PMCT and PMMR in the upper and lower lobe of the right lung
3 periphery were identified as pulmonary infarction with surrounding hemorrhage.

4 H&E staining of the wedge shaped lung lesions showed central infarcted necrotic lung
5 tissue and a surrounding hemorrhagic rim. Iron staining revealed iron positive
6 macrophages at the edge of necrotic lung tissue.

7 Furthermore, autopsy showed concentric hypertrophy of the heart (heart weight 520 g;
8 180 cm body length, 81 kg body weight) and an asymmetric heart configuration with a
9 hypertrophic right ventricle and round configuration of the apex. The large pulmonary
10 arteries were dilated and showed plaques indicative of pulmonary hypertension.

11 The manner of death was assessed as a natural death, the cause of death was
12 determined as right cardiac failure due to PTE.

13 **Discussion**

14 PMCT is widely used and accepted as a complementary examination to forensic
15 autopsy in routine forensic examination [3, 4]. Over the last 10 years, PMMR has been
16 introduced as an additional tool in post-mortem imaging mainly feasible for diagnosis
17 of soft tissue and organ pathology [5, 6]. Acute PTE is a frequently found natural cause
18 of death at autopsy [7]. However, pulmonary infarction accompanying PTE is a less
19 common finding. Pulmonary infarction presents mostly in patients with PTE and
20 reduced cardiac function or pre-existing pulmonary disease While PTE has been
21 demonstrated in PMCT and PMMR [5, 8–12], pulmonary infarction has neither been
22 shown nor discussed in PM-imaging.

23 Pulmonary infarction may present similarly to other pulmonary findings such as lung
24 cancer and infectious lung disease in CT imaging [13]. In clinical CT pulmonary

1 infarction is often described as wedge-shaped opacities located at the periphery of the
2 lung [14], also known as “Hampton’s hump” [15]. Hyperlucent focal areas may be
3 present within the infarction [16]. Pneumonia, cancerous pulmonary nodules or septic
4 emboli (Fig. 2) may also appear as pleura based, wedge shaped, inhomogeneous
5 lesions in clinical CT [17–19]. Distinction between these entities may therefore be
6 challenging or impossible [13]. Regarding cancerous pulmonary nodules, PMCT is
7 comparable to ante-mortem images in the early post-mortem interval [20]. In our case
8 we observed wedge-shaped, pleura-based lesions at the lung periphery mainly
9 appearing hyperdense with smaller hypodense areas in PMCT (Fig. 1). Thus, similar
10 appearance of pulmonary infarction in clinical CT and PMCT may be assumed.
11 However, since pulmonary infarction may not be distinguishable from infectious or
12 cancerous lung diseases, PMCT alone may not be enough to strengthen the diagnosis
13 of pulmonary infarction and additional PMMR of the lungs may be useful.

14 Combined appearance of PTE and wedge shaped lesions in post-mortem imaging may
15 hint to acute pulmonary infarction. Post-mortem clots in MRI usually show signs of
16 sedimentation due to gravitation with compartments of lower density containing fibrin
17 and compartments with higher density containing erythrocytes. The structure of vital
18 clots like PTE appears homogenous, with intermediate signal intensity on T2w images,
19 in direct contact with the vessel wall and situated within a hypointense layer of
20 sedimented erythrocytes [21]. Older pulmonary infarction may not be accompanied by
21 clear signs of PTE since previous acute PTE may present as strings and webs of
22 connective tissue [22] in the lumen of the pulmonary **arteries**, or may be complete
23 remnant free. In clinical contrast-enhanced CT-imaging, these strings are connected
24 to the vessel wall on both sides, surrounded by contrast media [23, 24]. As contrast-

1 enhanced imaging is not a routine tool in post-mortem imaging, the diagnosis of chronic
2 PTE will likely be established during autopsy.

3 Regarding pulmonary infarction Bray et al. [25] state that appearance of pulmonary
4 infarction in clinical magnetic resonance imaging varies according to the accumulated
5 aging blood within the alveoli and its signal characteristics. Therefore, blood in
6 hyperacute (less than 24 hours) pulmonary infarction areas appears hyperintense in
7 T2w and hypointense in T1w whereas the lesions appear hyperintense in T1w in the
8 acute interval (up to 1 week). In the presented case infarction areas appeared mainly
9 hyperintense with hypointense components in T2w and hypointense to isointense
10 containing small focal hypointense areas in T1w PMMR (Fig. 1). Based on the above-
11 mentioned characteristics this PMMR signal intensity corresponds to an infarction age
12 slightly over 24 hours. This is in accordance with the known case circumstances as
13 well as autptic and histologic findings. It can thus be assumed that in a short post-
14 mortem interval, characteristics of pulmonary infarction in PMMR correspond to those
15 in clinical MRI and may be applied for diagnosis and age determination of pulmonary
16 infarction. Literature regarding pulmonary findings in PMMR is scarce. To the best of
17 our knowledge, there is no literature describing scanning protocols in PMMR for
18 depiction of pulmonary infarction. Some of the faced difficulties in PMMR are rapid
19 changes in signal intensity in a post-mortem interval due to sedimentation,
20 decomposition as well as cooling of the corpse [26–28]. Knowing the temperature of
21 the body before scanning is of great importance, as the image contrast decreases for
22 both T1w and T2w images for lower body temperatures. At a body temperature below
23 20°C on T2w and below 10°C on T1w images, a visible decrease in image contrast
24 was observed [26].

1 Due to our in-house standard we used Dixon technique [29] for PMMR imaging. The
2 benefit of Dixon technique lies in the simultaneous generation of fat and water
3 suppressed images from a single acquisition. The Dixon in-phase sequences
4 correspond to T1w/T2w images seen in spin-echo sequences. However, fat and water
5 suppressed images are not crucial for identification of pulmonary infarctions. Since the
6 appearance of pulmonary infarction in PMMR seems to be similar to clinical MRI, it is
7 mainly dependent on the accumulated blood and its age characteristics. Therefore,
8 conventional T1 and T2 weighted spin-echo sequences will suffice.

9 **Conclusion**

10 Pleura based wedge shaped lesions in unenhanced PMCT may indicate pulmonary
11 infarction but lesions may not be distinguishable from other pulmonary pathologies.
12 Additional PMMR of the lungs using conventional T1 and T2 weighted sequences may
13 aid in diagnosis and age determination of pulmonary infarction at a short post-mortem
14 interval.

15

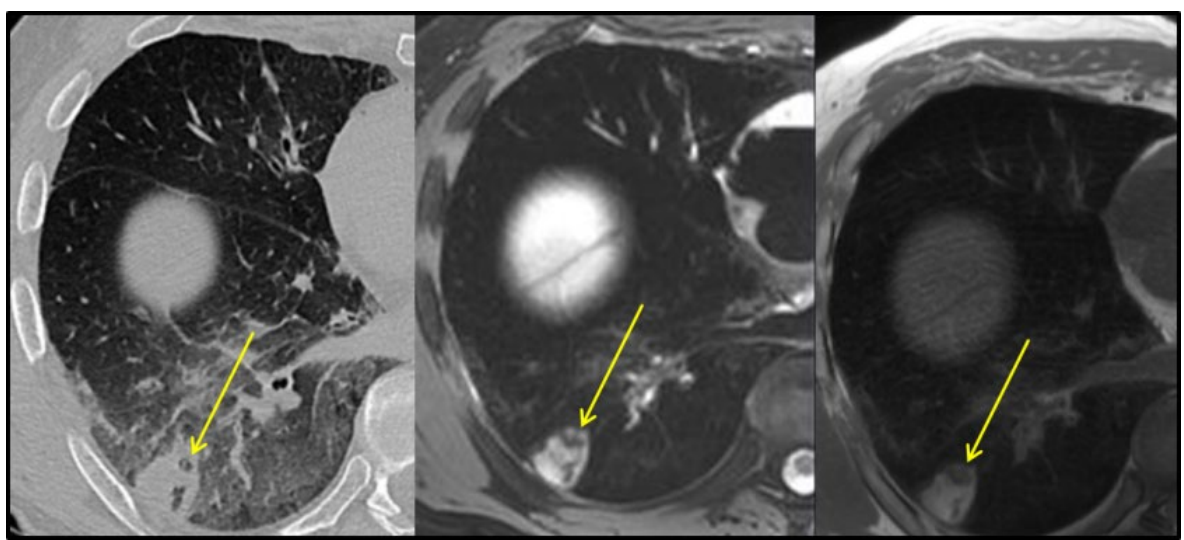
16

1 **Tables**

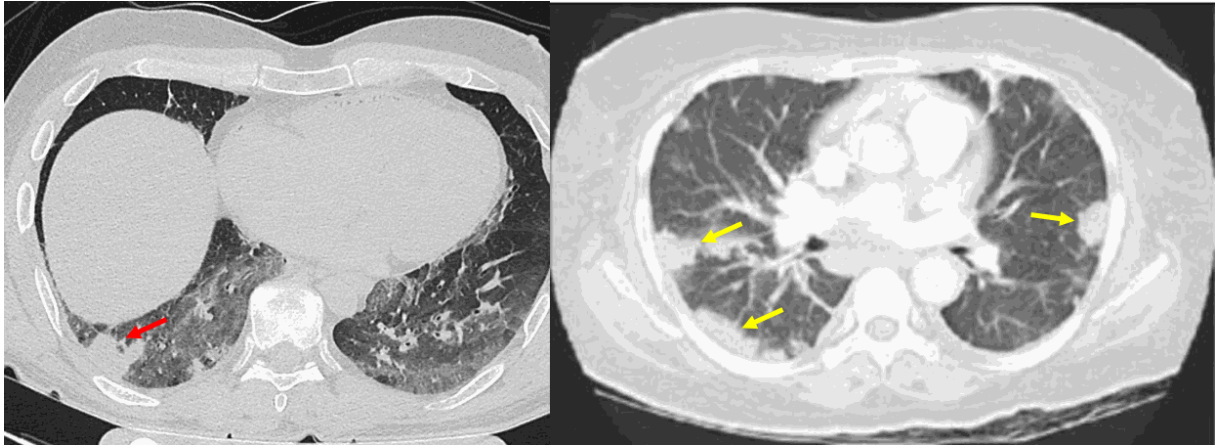
	In-phase	Out-of-phase	Fat only	Water only
T1w	iso- to hypointense	Iso- to hyperintense	lesion not visible	hyperintense
T2w	Iso- to hyperintense	Iso- to hyperintense	lesion not visible	hyperintense

2 Table 1
3 Appearance of pulmonary infarction in PMMR in T1w and T2w Dixon sequences
4

5 **Figures**



6
7 **Fig. 1:**
8 Axial PMCT (left image), axial in-phase T2w PMMR (middle image) and axial in-phase T1w PMMR (right image)
9 with exemplary wedge shaped lesion (yellow arrows) in the right lower lobe of the lung.
10
11
12
13
14
15
16
17
18
19



1

2 **Fig. 2:**

3 Depiction of undistinguishable wedge shaped pleura based lesions in PMCT and clinical CT. The left
4 image shows unenhanced PMCT with pulmonary infarction (red arrow). The right image shows
5 multiple, pleura based lesions due to septic emboli (yellow arrows) [19].

6

7

8

9 **Compliance with Ethical Standards**

10 This article does not contain any studies with live human participants or animals.

11 The authors declare that they have no conflicts of interest:

12 This work received no funding.

1 **References**

- 2 1. Jackowski C, Grabherr S, Schwendener N (2013) Pulmonary thrombembolism as cause
3 of death on unenhanced postmortem 3T MRI. *Eur Radiol* 23:1266–1270.
4 <https://doi.org/10.1007/s00330-012-2728-3>
- 5 2. (2000) Recommendation no. R (99) 3 of the Committee of Ministers to member states on
6 the harmonization of medico-legal autopsy rules. *Forensic Sci Int* 111:5–58
- 7 3. Willaume T, Farrugia A, Kieffer E-M, et al (2018) The benefits and pitfalls of post-
8 mortem computed tomography in forensic external examination: A retrospective study of
9 145 cases. *Forensic Sci Int* 286:70–80. <https://doi.org/10.1016/j.forsciint.2018.02.030>
- 10 4. Mishima S, Suzuki H, Fukunaga T, Nishitani Y (2018) Postmortem computed
11 tomography findings in cases of bath-related death: Applicability and limitation in
12 forensic practice. *Forensic Sci Int* 282:195–203.
13 <https://doi.org/10.1016/j.forsciint.2017.11.030>
- 14 5. Schwendener N, Jackowski C, Persson A, et al (2017) Detection and differentiation of
15 early acute and following age stages of myocardial infarction with quantitative post-
16 mortem cardiac 1.5T MR. *Forensic Sci Int* 270:248–254.
17 <https://doi.org/10.1016/j.forsciint.2016.10.014>
- 18 6. Mokrane F-Z, Savall F, Dercle L, et al (2017) Technical note: A preliminary comparative
19 study between classical and interventional radiological approaches for multi-phase post-
20 mortem CT angiography. *Forensic Sci Int* 271:23–32.
21 <https://doi.org/10.1016/j.forsciint.2016.12.008>
- 22 7. Micallef MJ (2018) The autopsy and diagnosis of pulmonary thrombo-embolism.
23 *Forensic Sci Med Pathol* 14:241–243. <https://doi.org/10.1007/s12024-018-9950-5>
- 24 8. Ruddy GN, Morgan B, Robinson C, et al (2017) Diagnostic accuracy of post-mortem CT
25 with targeted coronary angiography versus autopsy for coroner-requested post-mortem
26 investigations: a prospective, masked, comparison study. *Lancet Lond Engl* 390:145–
27 154. [https://doi.org/10.1016/S0140-6736\(17\)30333-1](https://doi.org/10.1016/S0140-6736(17)30333-1)
- 28 9. Harty MP, Harcke HT, Gould SW, Sukula-Perlman A (2018) Pulmonary embolus as
29 cause of death in an adolescent: demonstration on postmortem CT. *Pediatr Radiol*
30 48:745–748. <https://doi.org/10.1007/s00247-017-4041-4>
- 31 10. von Both I, Bruni SG, Herath JC (2018) Differentiation of antemortem pulmonary
32 thromboembolism and postmortem clot with unenhanced MRI: a case report. *Forensic*
33 *Sci Med Pathol* 14:95–101. <https://doi.org/10.1007/s12024-017-9940-z>
- 34 11. Ampanozi G, Held U, Ruder TD, et al (2016) Pulmonary thromboembolism on
35 unenhanced postmortem computed tomography: Feasibility and findings. *Leg Med*
36 *Tokyo Jpn* 20:68–74. <https://doi.org/10.1016/j.legalmed.2016.04.005>
- 37 12. Burke MP, Bedford P, Baber Y (2014) Can forensic pathologists diagnose pulmonary
38 thromboembolism on postmortem computed tomography pulmonary angiography? *Am J*
39 *Forensic Med Pathol* 35:124–131. <https://doi.org/10.1097/PAF.0000000000000086>

- 1 13. Gaeta M, Ascenti G, Mazziotti S, et al (2012) MRI differentiation of pneumonia-like
2 mucinous adenocarcinoma and infectious pneumonia. *Eur J Radiol* 81:3587–3591.
3 <https://doi.org/10.1016/j.ejrad.2011.12.022>
- 4 14. He H, Stein MW, Zalta B, Haramati LB (2006) Pulmonary infarction: spectrum of
5 findings on multidetector helical CT. *J Thorac Imaging* 21:1–7.
6 <https://doi.org/10.1097/01.rti.0000187433.06762.fb>
- 7 15. HAMPTON AO (1940) Correlation of postmortem chest teleroentgenograms with
8 autopsy findings, with special reference to pulmonary embolism and infarction. *Am J*
9 *Roentgen* 43:305–326
- 10 16. Miniati M (2016) Pulmonary Infarction: An Often Unrecognized Clinical Entity. *Semin*
11 *Thromb Hemost* 42:865–869. <https://doi.org/10.1055/s-0036-1592310>
- 12 17. Rosado-de-Christenson ML, Abbott GF, McAdams HP, et al (2003) From the Archives
13 of the AFIP. *RadioGraphics* 23:759–783. <https://doi.org/10.1148/rg.233025165>
- 14 18. Luciano C, Francesco A, Giovanni V, et al (2011) CT signs, patterns and differential
15 diagnosis of solitary fibrous tumors of the pleura. *J Thorac Dis* 2:21–25–25
- 16 19. Pictorial essay of radiological features of benign intrathoracic masses.
17 <https://www.ncbi.nlm.nih.gov/pmc/articles/PMC4652288/>. Accessed 22 Nov 2019
- 18 20. Ikeda G, Yamamoto R, Suzuki M, et al (2007) Postmortem computed tomography and
19 magnetic resonance imaging in a case of terminal-stage small cell lung cancer: an
20 experience of autopsy imaging in tumor-related death. *Radiat Med* 25:84–87.
21 <https://doi.org/10.1007/s11604-006-0104-4>
- 22 21. Jackowski C, Thali M, Aghayev E, et al (2006) Postmortem imaging of blood and its
23 characteristics using MSCT and MRI. *Int J Legal Med* 120:233–240.
24 <https://doi.org/10.1007/s00414-005-0023-4>
- 25 22. Pulmonary Arterial Bands and Webs; an Unrecognized Manifestation of Organized
26 Pulmonary Emboli. <https://www.ncbi.nlm.nih.gov/pmc/articles/PMC1949576/>. Accessed
27 14 Nov 2019
- 28 23. Castañer E, Gallardo X, Ballesteros E, et al (2009) CT Diagnosis of Chronic Pulmonary
29 Thromboembolism. *RadioGraphics* 29:31–50. <https://doi.org/10.1148/rg.291085061>
- 30 24. Chronic pulmonary embolism: diagnosis.
31 <https://www.ncbi.nlm.nih.gov/pmc/articles/PMC6039808/>. Accessed 14 Nov 2019
- 32 25. Bray TJP, Mortensen KH, Gopalan D (2014) Multimodality imaging of pulmonary
33 infarction. *Eur J Radiol* 83:2240–2254. <https://doi.org/10.1016/j.ejrad.2014.07.016>
- 34 26. Ruder TD, Hatch GM, Siegenthaler L, et al (2012) The influence of body temperature on
35 image contrast in post mortem MRI. *Eur J Radiol* 81:1366–1370.
36 <https://doi.org/10.1016/j.ejrad.2011.02.062>
- 37 27. Ruder TD, Thali MJ, Hatch GM (2014) Essentials of forensic post-mortem MR imaging
38 in adults. *Br J Radiol* 87:. <https://doi.org/10.1259/bjr.20130567>

1 28. Wagenveld IM, Blokker BM, Wielopolski PA, et al (2017) Total-body CT and MR
2 features of postmortem change in in-hospital deaths. PLoS ONE 12:.
3 <https://doi.org/10.1371/journal.pone.0185115>

4 29. Dixon WT (1984) Simple proton spectroscopic imaging. Radiology 153:189–194.
5 <https://doi.org/10.1148/radiology.153.1.6089263>

6

7